Journal of Catalysis 260 (2008) 7–16

Contents lists available at ScienceDirect

Journal of Catalysis

www.elsevier.com/locate/jcat

# Effect of K promotion of Fe and FeMn Fischer–Tropsch synthesis catalysts: Analysis at the site level using SSITKA

Nattaporn Lohitharn, James G. Goodwin Jr.*

*Department of Chemical and Bimolecular Engineering, Clemson University, Clemson, SC 29634, USA*

ARTICLE INFO

*Article history:*
Received 12 April 2008
Revised 12 August 2008
Accepted 24 August 2008
Available online 1 October 2008

*Keywords:*
Fischer–Tropsch synthesis (FTS)
CO hydrogenation
Methanation
Steady-state isotopic transient kinetic analysis (SSITKA)
Mn promotion
K promotion
Water–gas shift (WGS)
Fe-based FTS catalysts

ABSTRACT

Promoting a precipitated $FeCuSiO_2$ catalyst with Mn has been shown to significantly improve its catalytic activity for Fischer–Tropsch synthesis (FTS). Although the impact of K promotion on the activity of Fe catalysts with and without Mn addition has been studied previously, no one has previously delineated how K influences the concentration of active surface intermediates and the intrinsic site activities of Fe and, more specifically, Mn-promoted Fe catalysts. This paper addresses that issue using steady-state isotopic transient kinetic analysis (SSITKA). Adding K at relatively low concentrations to the base Fe and Mn-promoted Fe catalysts improved the catalyst activity, but the activity of the catalysts declined with the addition of an excess amount. The percentage of light olefins ($C_2$–$C_4$ fraction) and chain growth probability ($\alpha$) were enhanced, as expected with the presence of K, regardless of Mn addition. The addition of K decreased the BET surface area and the concentration of surface exposed $Fe^0$ atoms (as determined by CO chemisorption). The intrinsic site activities ($TOF_{ITK}$) of all of the Fe catalysts determined using SSITKA were essentially identical, regardless of the concentration of added K or Mn promotion. This indicates that adding K to unpromoted or Mn-promoted Fe catalysts did not greatly affect the activity of the active sites. Rather, the higher catalyst activities observed for the Fe and Mn-promoted Fe catalysts with K addition were due primarily to an increase in the number of active surface intermediates leading to hydrocarbon products.



## 1. Introduction

Fischer–Tropsch synthesis (FTS) is a well-known reaction and has been used commercially for more than 70 years. The synthesis involves the hydrogenation of CO to high-value liquid hydrocarbon fuels and chemical products [1]. The use of biomass and coal as raw materials for FTS is of great interest due to $CO_2$ (a greenhouse gas) recycling and the existence of large coal reserves in the United States, respectively [2]. However, syngas derived from biomass or coal has a $H_2/CO$ ratio significantly below 2 (the ratio needed for hydrocarbon synthesis); thus, a high water–gas shift (WGS) activity catalyst is required to provide additional $H_2$ for the reaction. Bulk Fe catalysts are particularly useful for syngas with low $H_2/CO$ ratios due to their high WGS activity and low cost, although they are less active for FTS than Co-based catalysts [3].

A number of studies have indicated an improved activity and/or selectivity on the addition of transition metals to Fe-based FTS catalysts [4–7]. Our previous work showed that the addition of various transition metals besides Cu, such as Zr, Cr, Mo, Mn, Ta and V, greatly increased the catalyst activities for both CO hydrogenation and WGS activity in varying degrees [8]. The addition of moderate amounts of Mn has been found to promote the activity of Fe catalysts [8,9], the formation of low-molecular weight olefins [4,5,8,9], higher hydrocarbon formation [10], and catalyst stability [4]. In addition, promotion of an Fe catalyst with small amounts of Mn has been shown to improve the surface basicity and carburization of Fe [9,10].

The impact of K addition on the performance of Fe FTS catalysts has been studied extensively and is well established. K is known to promote the formation of olefins and longer-chain hydrocarbon molecules, the carburization of surface Fe, and the suppression of $CH_4$ formation [1,3,11–13]. K promotion strengthens the Fe–C bond by increasing the electron density on Fe while weakening Fe–H and C–O bonds [13–15]. The positive impact of K addition on the activity of Fe catalysts depends on the level of promotion [1,3,11–13]. Enhanced WGS activity of Fe catalysts on K promotion also has been observed [11,12]. A similar impact of K promotion has been reported for FeMn catalysts [10,11,16].

To date, no study has investigated the impact of K on the surface kinetic properties (at the site level) of Fe and Mn-promoted Fe catalysts for CO hydrogenation. In the present study, steady-state isotopic transient kinetic analysis (SSITKA) was carried out to determine the surface kinetic parameters at the site level of K-promoted $FeCuSiO_2$ bulk catalysts with and without Mn addition.

* Corresponding author. Fax: +1 (864) 656 0784.
*E-mail address:* jgoodwi@clemson.edu (J.G. Goodwin Jr.).

0021-9517/$ – see front matter 
doi:10.1016/j.jcat.2008.08.011

In a previous study [8], an Fe catalyst promoted with Mn with a formulation of 80Fe/20Mn/5Cu/17$SiO_2$ was reported to give rise to the highest catalyst activity among various Fe catalysts with added transition metals; thus, this formulation was used in the present study for the Mn-promoted Fe catalyst. The impact of varying K concentration on the activity of the Fe and Mn-promoted Fe catalysts also was investigated.

## 2. Experimental

### 2.1. Catalyst preparation

Catalysts were prepared using a pH precipitation technique [17], according to the general formulation 100Fe/5Cu/17Si/*x*K and 80Fe/20Mn/5Cu/17Si/*x*K (on a relative atomic basis, where Fe + Mn = 100), with $x \leqslant 9$. The details of catalyst preparation used in this study can be found elsewhere [8]. In brief, a solution containing $Fe(NO_3)_3{\cdot}9H_2O$, $CuN_2O_6{\cdot}3H_2O$, $Si(OC_2H_5)_4$ with and without $Mn(NO_3)_2$ for Mn-promoted Fe (FeMn) and unpromoted Fe (100Fe) catalysts, respectively, was precipitated with $NH_4OH$ at 83 °C until the precipitate had a pH of 8–9. The precipitate was aged at room temperature for 17 h, then washed thoroughly with deionized water to eliminate excess $NH_4OH$. The washed precipitate was dried at 110 °C for 18–24 h and then sieved to <90 μm before being calcined in air at 300 °C for 5 h. In the case of K promotion, after sieving, the Fe catalysts were impregnated to incipient wetness with a $KHCO_3$ solution to give the desired K content. Subsequently, the catalysts were dried at 110 °C for 4 h before calcination at 300 °C.

Catalyst nomenclatures used are 100Fe, 100Fe*x*K, FeMn, and FeMn*x*K for the benchmark catalyst, the K-promoted Fe catalyst at *x* at% (relative to the amount of Fe), the Mn-promoted Fe catalyst with 20 at% (relative to the amount of Fe + Mn) of Mn, and the K-promoted FeMn catalysts with 20 at% of Mn and *x* at% (relative to the amount of Fe + Mn) of K, respectively. General catalyst nomenclatures for K-promoted Fe and K-promoted FeMn catalysts are 100FeK and FeMnK, respectively.

### 2.2. Catalyst characterization

#### 2.2.1. BET surface area

The BET surface areas of catalysts were analyzed by $N_2$ physisorption using a Micromeritics ASAP 2020 automated system. A 0.3-g sample was degassed under a vacuum of $10^{-3}$ mm Hg at 100 °C for 1 h, after which the temperature was ramped to 300 °C (at 10 °C/min) and held for 2 h before $N_2$ physisorption at 77 K.

#### 2.2.2. Catalyst composition

The metal composition of the freshly calcined catalysts and carbon content of spent catalysts were analyzed using inductively coupled plasma optical emission spectrometry (ICP-OES) and a combustion method, respectively, by Galbraith Laboratories Inc. (Knoxville, TN). Carbon content of the spent Fe catalysts was determined after the catalyst was passivated with 40 $cm^3$/min of 2% $O_2$ in He at room temperature. During passivation, the temperature increased about 7 °C before decreasing back to room temperature, indicating completion of passivation.

#### 2.2.3. X-Ray diffraction (XRD)

The crystallinity of prepared catalysts was studied using a Scintag 2000 X-ray diffractometer with monochromatized Cu$K_\alpha$ radiation (40 kV, 40 mA) and a Ge detector. A step scan mode was used with a scan rate of 0.02° (2$\theta$) per second from 10 to 90°.

#### 2.2.4. Scanning electron microscopy (SEM) and energy dispersive X-ray spectroscopy (EDX)

The catalyst morphologies were studied using SEM. The elemental distributions on the surface of catalyst particles were determined using EDX. SEM and EDX were performed using a Hitachi FESEM-S4800 in the scanning electron (SE) mode. The accelerating voltage was 20 kV, with a working distance of 15 mm.

#### 2.2.5. Temperature-programmed reduction

The reducibility of Fe was determined by $H_2$ temperature-programmed reduction (TPR) using an Altamira AMI-1 system. A 0.1-g sample of the calcined catalyst was reduced in 5% $H_2$/Ar (30 $cm^3$/min) as the temperature was increased from 35 to 800 °C at a rate of 2 °C/min. A thermal conductivity detector (TCD) was used to measure $H_2$ consumption, and the detector output was calibrated based on 100% reducibility of $Ag_2O$ powder. A $H_2O$ trap was placed before the TCD.

#### 2.2.6. CO chemisorption

CO chemisorption was performed using a Micromeritics ASAP 2010 automated system to determine the number of active surface metal atoms. Before CO chemisorption, 0.1 g of the calcined catalyst was first evacuated to $10^{-6}$ mm Hg at 100 °C for 30 min, and then reduced under flowing $H_2$ at 280 °C for 12 h (at a ramp rate of 2 °C/min). The catalyst was evacuated at 280 °C for 60 min to desorb any $H_2$. The analysis was carried out at 35 °C. An average CO:$Fe_s$ stoichiometry of 1:2 was assumed [18].

### 2.3. Kinetic measurements

Catalytic measurements were carried out in a quartz microreactor (8 mm i.d.). The reaction conversion was kept below 10% (differential reaction conditions) to minimize temperature and concentration gradients. A 10–50 mg catalyst sample was reduced *in situ* at 280 °C (after heating to that temperature at a rate of 2 °C/min) under 30 $cm^3$/min of $H_2$ (National Specialty Gases, Zero Grade) for 12 h. Then 30 $cm^3$/min of He (National Specialty Gases, UHP) was used to purge the catalyst for 15 min before the reaction at 280 °C and a constant pressure of 1.8 atm. The total flow rate of the reaction mixture was kept constant at 60 $cm^3$/min (STP) and contained 5 $cm^3$/min of 95% CO + 5% Ar (National Specialty Gases), 10 $cm^3$/min of $H_2$, and balance He to obtain a $H_2$:CO ratio of 2:1. The reaction line and sampling valves were maintained at 200 °C with heating tapes to avoid condensation of higher hydrocarbon products. The effluent samples were analyzed using a Varian 3700 gas chromatograph equipped with a AT-Q 30 m × 0.53 mm Heliflex capillary column with a flame ionization detector (FID) for hydrocarbon detection and with a Carbosphere 80/100 6′ × 1/8″ × 0.085″ SS packed column with a TCD for CO and $CO_2$ detection. All experiments were reproducible within a maximum error of ±5%.

### 2.4. Steady-state isotopic transient kinetic analysis

During SSITKA measurements, a switch between 95% $^{12}CO$ + 5% Ar (National Specialty Gases) and $^{13}CO$ (Isotec, 99%) was made by using a Valco 2-position valve with an electric actuator without disturbing any other reaction conditions (i.e., the total flow rate and reaction pressure of these 2 feed streams were kept identical during the switch). The gas-phase holdup for the reaction system was measured by the presence of a small amount of Ar in the unlabeled $^{12}CO$ stream. The reaction was carried out at the same conditions as stated above, but with a $H_2$:CO ratio of 20:1 to obtain $CH_4$ as the primary product (i.e., the total flow rate of the reaction mixture was 1 $cm^3$/min of 95% CO + 5% Ar, 20 $cm^3$/min of $H_2$, and 39 $cm^3$/min of He). The effluent gas was analyzed online

**Table 1**
Results from BET, TPR and CO chemisorption for the various Fe-based catalysts

| Catalyst[a] | BET S.A.[b] ($m^2/g$) | $H_2$-TPR | | CO chemisorption | |
|---|---|---|---|---|---|
| | | Peak temperature[b] (°C) | %Fe reducibility[c] | Total CO chemisorbed[d] (μmol/g) | %Fe dispersion[e] |
| 100Fe | 329 | 220 | 35 | 119 | 2.7 |
| 100Fe1.5K | 351 | 228 | 34 | 72 | 1.6 |
| 100Fe2.5K | 337 | 227 | 35 | 91 | 2.0 |
| 100Fe4K | 298 | 237 | 31 | 118 | 2.6 |
| 100Fe9K | 289 | 259 | 27 | 73 | 1.6 |
| FeMn | 381 | 278 | 32 | 141 | 3.2 |
| FeMn2.5K | 370 | 273 | 31 | 96 | 2.2 |
| FeMn4K | 356 | 273 | 33 | 108 | 2.4 |
| FeMn6.5K | 322 | 280 | 32 | 128 | 2.9 |
| FeMn9K | 305 | 283 | 27 | 66 | 1.5 |

[a] All catalysts also contained 5Cu and 17Si.
[b] Max error = ±5%.
[c] %Fe reduced in first TPR peak. Equivalent to %Fe reduced during standard reduction. Max error = ±5%.
[d] Determined by extrapolating the total chemisorption isotherm to zero pressure. Max error = ±5%. Most measurements were repeated.
[e] Based on total CO chemisorbed, $CO/Fe_s = 0.5$, % dispersion = 2 × total CO chemisorbed/total number of Fe atoms. Max error = ±7%.

by gas chromatography and mass spectrometry using a Balzers–Pfeiffer Prisma 200-amu quadrupole mass spectrometer (Pfeiffer Vacuum) via a 1/16-inch capillary tube with differential pumping. The gas inlet line to the mass spectrometer was heated to 120 °C to avoid the deposition of heavy hydrocarbon products and was designed to be as short as possible to minimize gas phase holdup in the system. The mass spectrometer was equipped with a high-speed data-acquisition system interfaced to a personal computer using Balzers Quadstar 422 v 6.0 software (Balzers Instruments). Surface kinetic parameters, including the average surface residence time of $CH_4$ and of CO ($\tau_{CH_4}$ and $\tau_{CO}$) and the surface concentrations of $CH_x$ (leading to $CH_4$) and of CO ($N_{CH_4}$ and $N_{CO}$), were determined from the isotopic transients using SSITKA data analysis software [19,20].

## 3. Results and discussion

### 3.1. Catalyst characterization

#### 3.1.1. BET surface area

BET surface areas of various Fe catalysts are shown in Table 1. The addition of Mn appeared to increase the BET surface area of the Fe catalysts (as has been shown previously [21]). Promotion with larger amounts of K, on the other hand, decreased the BET surface area of the Fe catalysts somewhat, regardless of Mn promotion. An effect of K on the loss of surface area also has been reported elsewhere [3,11]. Dry [3] has suggested that strong bases like K can decrease the surface area of the Fe catalyst by increasing the Fe crystallite size. In the present case, K was added to the Fe and FeMn catalysts after precipitation. In these catalysts, the impact of K promotion on the surface area was not very significant due to the presence of the $SiO_2$ structural promoter, which induces a large initial BET surface area.

#### 3.1.2. XRD

The XRD peaks (not shown) for the fresh calcined catalysts were very broad, suggesting that all of the oxide phases of Fe, Mn, K, or Cu were XRD amorphous or contained only crystallites of small size.

#### 3.1.3. SEM and EDX

Morphologies of the fresh calcined 100Fe, 100Fe4K, FeMn, and FeMn4K catalysts observed using SEM are shown in Figs. 1a, 1b, 1c, and 1d, respectively. No difference in particle morphologies among the catalysts with different concentrations of K promotion was found; however, it appears that the average granule size of FeMn (10–60 μm) and FeMnK (15–60 μm) was smaller than that of 100Fe (20–70 μm) and 100Fe4K (40–100 μm). Based on the XRD results, it is apparent that the catalyst granules detected by SEM would have been composed of thousands of very small Fe oxide crystallites bound together by the $SiO_2$ structural promoter, known to prevent the sintering of $Fe_2O_3$ crystallites [3]. In addition, EDX mapping, as shown in Fig. 2 for 100Fe4K, revealed that the elements were well distributed on the granule surfaces of the catalysts with no obvious segregation.

#### 3.1.4. TPR

The reduction behaviors of the Fe catalysts as determined using $H_2$-TPR are shown in Figs. 3a and 3b for 100FeK and FeMnK, respectively. Based on the similar TPR profile for all of the Fe catalysts to that of pure $Fe_2O_3$ powder (reference), it can be inferred that $Fe_2O_3$ was the primary Fe phase of the fresh calcined catalysts but was reduced at lower temperatures due to Cu promotion [1,22].

All Fe catalysts showed two distinct peaks at 215–280 °C and 600 °C, which have been assigned to the reduction of $Fe_2O_3 \rightarrow Fe_3O_4$ and $Fe_3O_4 \rightarrow Fe$, respectively [23,24]. A previous study [8] has shown that the first reduction step given by the first TPR peak at around 215–280 °C is obtained when the temperature is held at 280 °C for 12 h (the standard reduction procedure before reaction). Thus, because the catalysts exhibited initial activity after the standard reduction, it seems likely that some reduction of $Fe_2O_3$ to Fe metal or FeO also must have occurred during the standard reduction procedure and, consequently, during the first TPR peak. Reporting the percent reducibility of Fe based on the entire TPR profile (ramping the temperature from room temperature up to 800 °C) would greatly overestimate the degree of reducibility of the catalysts used in the reaction studies. In addition, because the catalysts prepared in this study contain multiple metal oxides that also can be reduced, determination of the absolute %Fe reducibility for this complex catalyst system is difficult. Thus, the %Fe reducibility reported in Table 1 was calculated based only on the first TPR peak and the assumption that the reduction of $Fe_2O_3 \rightarrow$ Fe occurs without including any reduction of CuO or MnO.

A significant delay in the first reduction peak temperature was observed for FeMn compared with the base 100Fe catalyst, possibly due to the ability of MnO to stabilize $Fe^{2+}$ [16,26,27] and/or the difficult migration of Fe cations to the catalyst surface in the presence of $Mn_3O_4$ [26]. Adding K at low concentrations to 100Fe and FeMn had little if any impact on the first reduction peak temperature (Fig. 3) or %Fe reducibility (Table 1). However, higher loadings of K appeared to slightly decrease the reducibility of Fe and cause

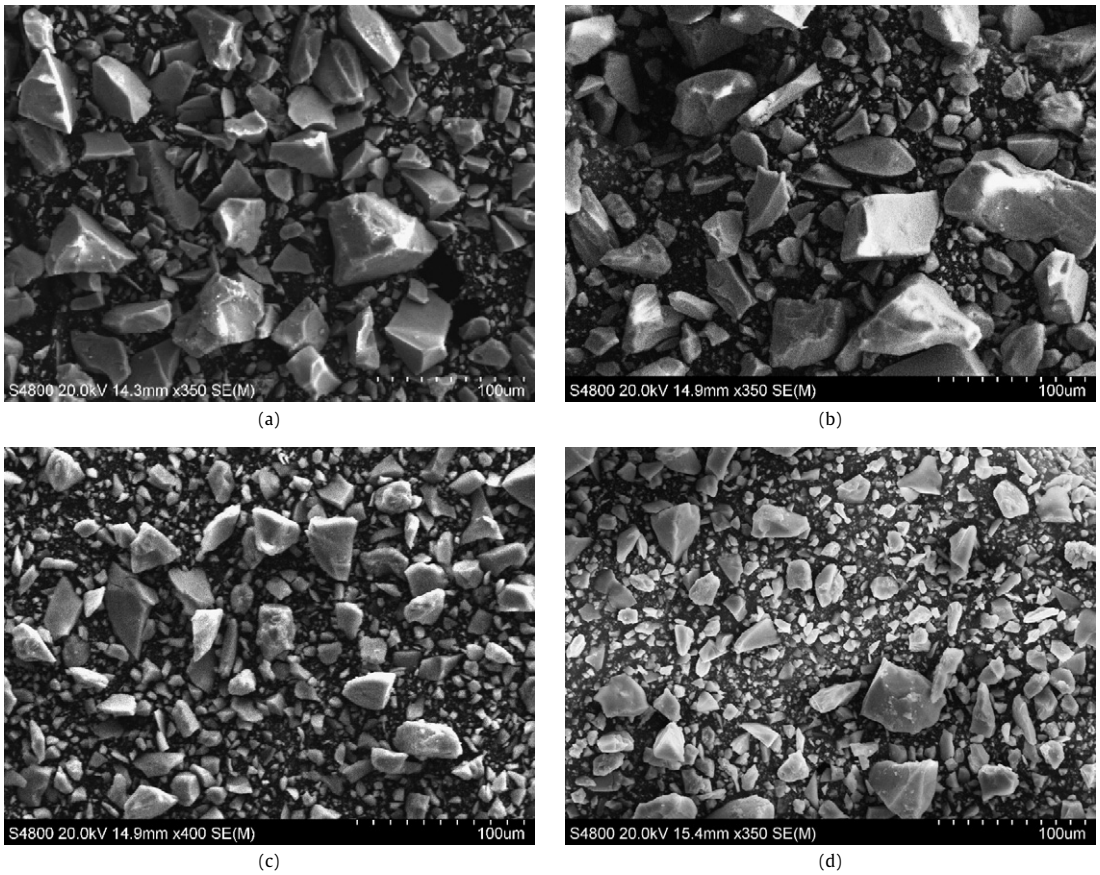


**Fig. 1.** SEM micrographs of calcined (a) 100Fe, (b) 100Fe4K, (c) FeMn, and (d) FeMn4K.

a slight shift in the first TPR peak to higher temperature. Rankin and Bartholomew [25] have suggested that the interaction of Fe oxide and K oxide could cause a delay in the reduction of Fe due to the suppressed adsorption of $H_2$.

### 3.1.5. CO chemisorption

The total amounts of CO chemisorbed and %Fe dispersion are shown in Table 1. The impact of K addition on the total amounts of CO chemisorbed and, consequently, %Fe dispersion for the 100Fe and FeMn catalysts is not obvious. However, it appears that K promotion of Fe and FeMn catalysts did not improve the dispersion of Fe within experimental error. K species may have covered some surface Fe atoms, resulting in lower total CO chemisorbed.

## 3.2. Catalyst activity

### 3.2.1. Fischer–Tropsch synthesis

A previous study [8] found no heat or mass transfer limitations for the 100Fe and FeMn catalysts under the reaction conditions used here. The activities of 100Fe and FeMn catalysts with K promotion are shown in Figs. 4 and 5, respectively. The activity of 100Fe for hydrocarbon production was significantly promoted during the induction period by the addition of K to varying degrees, depending on K content (Fig. 4a). The optimum performance was achieved for the catalyst with 1.5 at% K (relative to Fe), considering both maximum activity and TOS activity. Higher loadings of K resulted in lower activity maxima and greater deactivation, especially for 100Fe9K. On the other hand, the activity of Fe catalysts for $CO_2$ formation increased monotonically with increasing K content (Fig. 4b). The steady-state formation rate of $CO_2$ for 100FeK was at least twice as great as that observed for the benchmark 100Fe catalyst.

The activities of the K-promoted FeMn catalysts for CO hydrogenation and $CO_2$ formation are shown in Figs. 5a and 5b, respectively. As has also been shown previously, the addition of Mn to the Fe catalyst significantly enhanced the Fe activities for both CO hydrogenation and $CO_2$ formation. The TOS activity of FeMn was reasonably stable and was almost twice that of 100Fe at 6 h TOS. The promotion of the FeMn catalyst with K resulted in catalysts with even greater activities. The initial formation rate of hydrocarbon products of the K-promoted FeMn was at least 3 times greater than that of the unpromoted Fe catalyst (100Fe) and showed almost no induction period of reaction. The initial activity of Fe catalysts for the $CO_2$ formation, as shown in Fig. 5b, was improved considerably by the presence of Mn and K. FeMnK exhibited no induction period for $CO_2$ formation, with a formation rate at least 4 times greater than that of the benchmark catalyst (100Fe).

The different behaviors of the Fe catalysts in terms of induction periods for CO hydrogenation and for the formation of $CO_2$ product suggest the presence of different types of active sites/Fe phases. It has been strongly suggested that $Fe_3O_4$ is the active Fe phase for the WGS reaction [28], whereas Fe carbides are the active phase for FTS [29–31]. The existence of an induction period for FTS may be due to the need to convert $\alpha$-Fe to Fe carbides [30]. Enhanced carburization of Fe with the addition of K or Mn, as has been suggested [9,10,32], could explain the greater initial activity observed on the addition of K or Mn.

Maximum and steady-state catalyst activities with relative K loading are plotted in Figs. 6a and 6b for the Fe-based catalysts without and with Mn addition, respectively. Both the maximum and steady-state activities of 100Fe for $CO_2$ formation increased with increasing K content, whereas the activities of 100Fe for CO hydrogenation went through a maximum for K promotion at 1.5 at% (relative to Fe) (Fig. 6a). The formation of $CO_2$ and hydro-

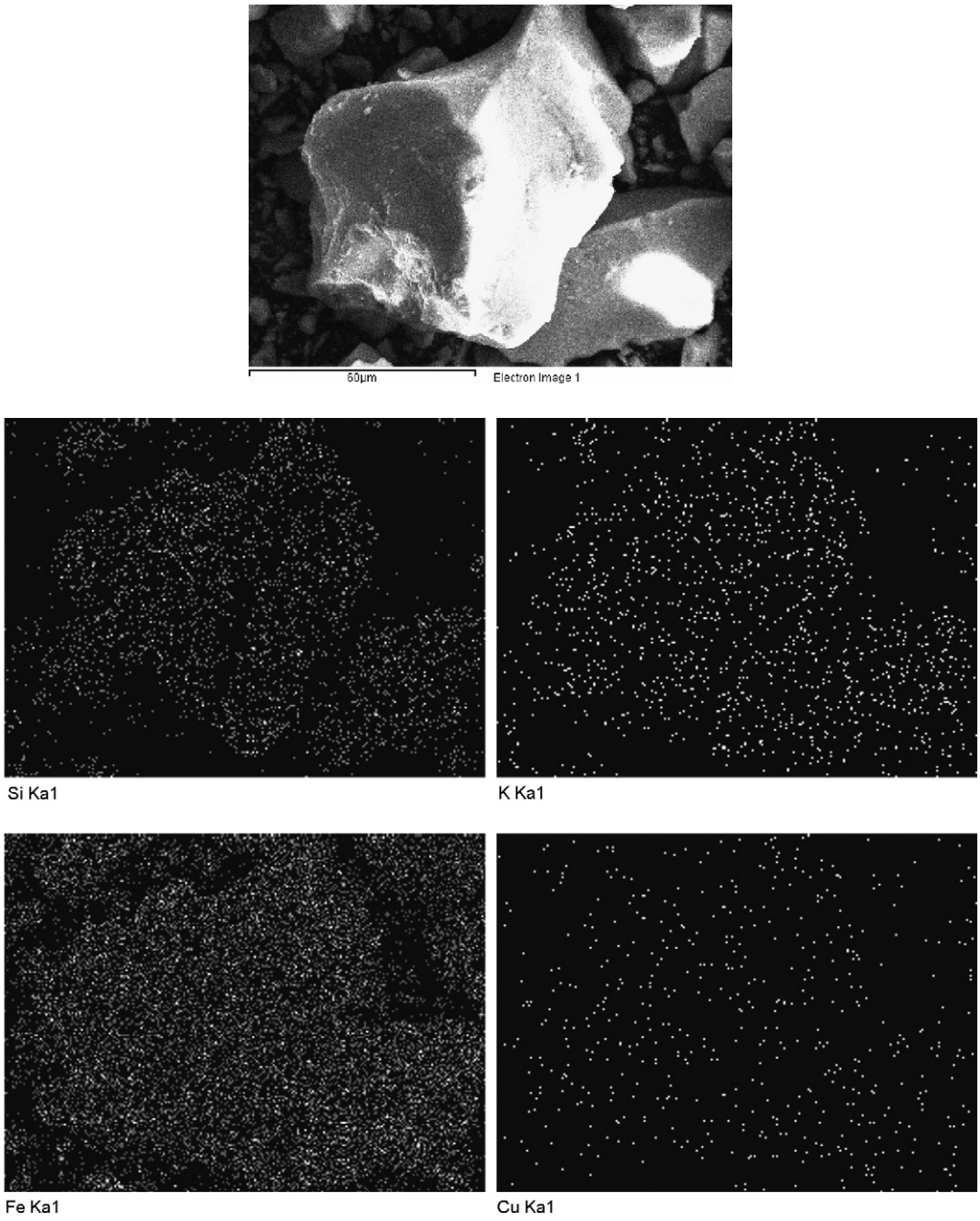


**Fig. 2.** EDX mapping of the surface of a calcined 100Fe4K particle.

carbon products for FeMn also increased with increasing K content, but with optimum activities at 6.5 at% K (relative to Fe + Mn). The activities of the FeMn catalysts declined with increasing K promotion (Fig. 6b).

For most of the catalysts, significantly more $CO_2$ than total hydrocarbon products was produced at the maximum activity. Given the CO hydrogenation reaction and the WGS reaction shown in Eqs. (1) and (2), respectively, and assuming that every $H_2O$ molecule produced underwent the WGS reaction, the resulting amount of $CO_2$ should have been equal to the number of moles of carbon contained in the hydrocarbon products.

CO hydrogenation:

$$CO + 2H_2 \rightarrow -CH_2- + H_2O, \quad (1)$$

WGS reaction:

$$CO + H_2O \rightarrow CO_2 + H_2, \quad (2)$$

Boudouard reaction:

$$2CO \rightarrow CO_2 + C. \quad (3)$$

Because this was not the case, the excess amount of $CO_2$ detected during the initial stage of reaction must have been formed via the Boudouard reaction. Based on Eq. (3), for each excess mole of $CO_2$ formed (greater than the amount of carbon in hydrocarbons), 1 mol of carbon is deposited on the catalyst in the form of Fe carbides and/or inactive carbon.

The impact of K promotion on the Boudouard activity of Fe catalyst can be estimated by determining the area between the $CO_2$ and the total hydrocarbon formation rate curves (Figs. 4 and 5, respectively). The calculated values for the amount for carbon de-

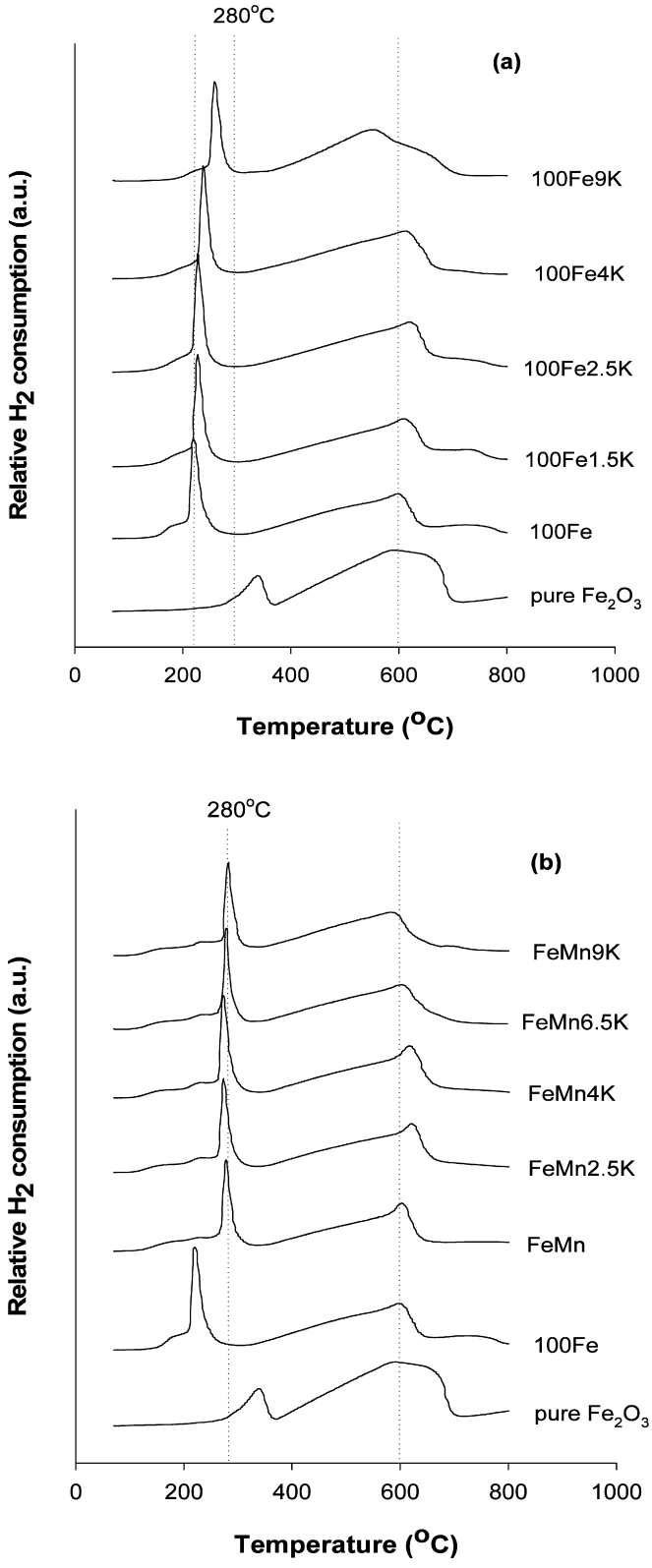


**Fig. 3.** TPR profiles of the fresh calcined (a) K-promoted 100Fe catalysts and (b) K-promoted FeMn catalysts.

position via the Boudouard reaction, as well as the total amount of carbon deposition obtained via elemental analysis by Galbraith, are given in Table 2. The table clearly shows that the amount of carbon deposition (based on the amount estimated via the Boudouard reaction and the amount determined by elemental analysis) increased with increasing K content, regardless of whether or not the Fe catalysts were promoted by Mn.

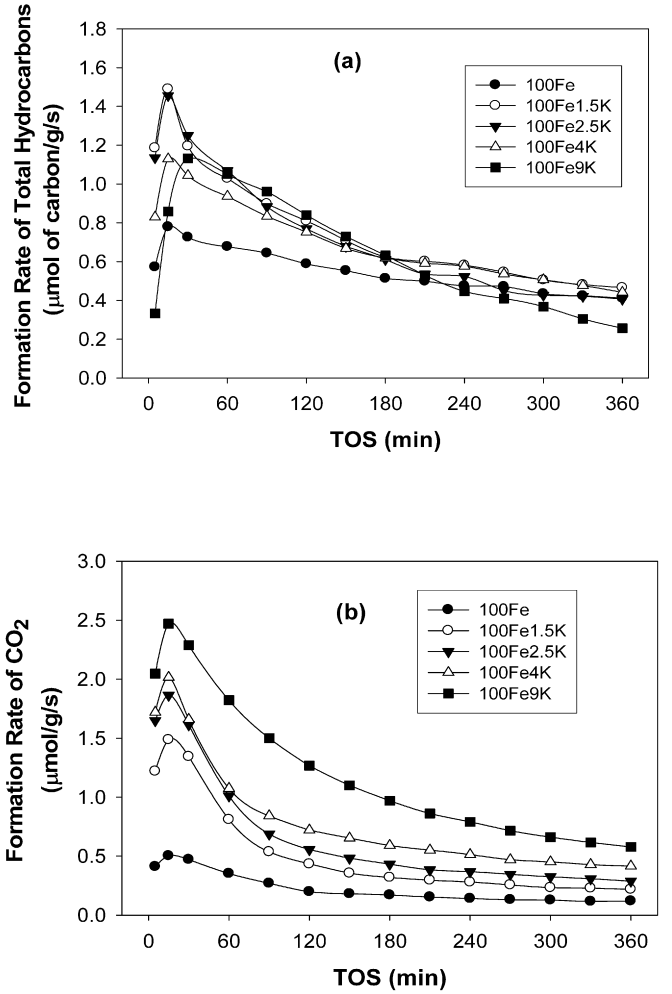


**Fig. 4.** Formation rates of (a) total hydrocarbons ($C_1$–$C_8$) and (b) $CO_2$ for the K-promoted Fe catalysts.

The total carbon deposited, as determined by elemental analysis, can be in the form of Fe carbides and/or coke. In this case, if all of the Fe formed $\chi$-$Fe_2C_5$ (as has been suggested to be the major Fe active carbide phase for FTS [30]), then the amount of inactive carbon in the form of coke can be estimated (as reported in Table 2). It can be seen that the amount of coke formation also increased with increasing K content for both 100Fe and FeMn catalysts. Adding K in higher concentrations significantly promoted the activity of the Fe catalysts for the Boudouard reaction and coke formation. The 100Fe9K catalyst had the most inactive carbon (coke) deposited more than FeMn9K (at relatively the same K content). This is the likely reason for the greater catalyst deactivation seen for 100Fe9K (see Fig. 4a).

A summary of reaction rates, % hydrocarbon selectivities on a carbon basis, % light $C_2$–$C_4$ olefin fractions and chain growth probabilities ($\alpha$) of the various Fe catalysts is shown in Table 3. $\%CH_4$ selectivity significantly decreased while % selectivities for $C_5$–$C_8$ hydrocarbons increased with increasing amount of K added (no hydrocarbons > $C_8$ were produced in significant concentrations to be detectable by gas chromatography under differential reaction conditions). % Light olefin ($C_2$–$C_4$) formation and $\alpha$ also increased with increasing K content. % Light olefin ($C_2$–$C_4$) selectivity was nearly 100% of that fraction, while $\alpha$ increased up to 0.63, as expected [3].

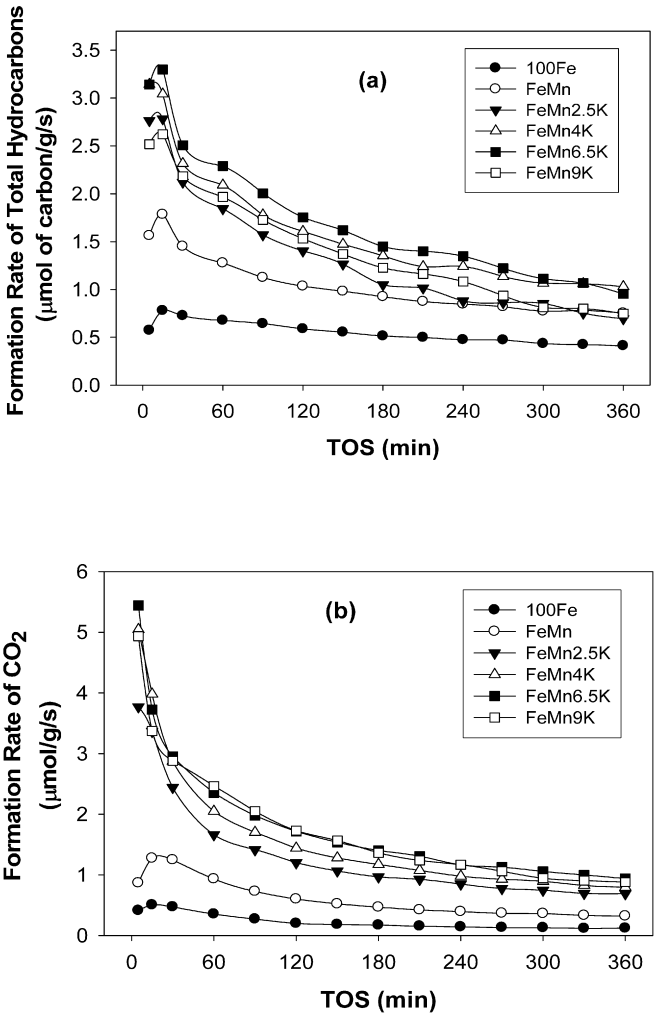


**Fig. 5.** Formation rates of (a) total hydrocarbons ($C_1$–$C_8$) and (b) $CO_2$ for the K-promoted FeMn catalysts.

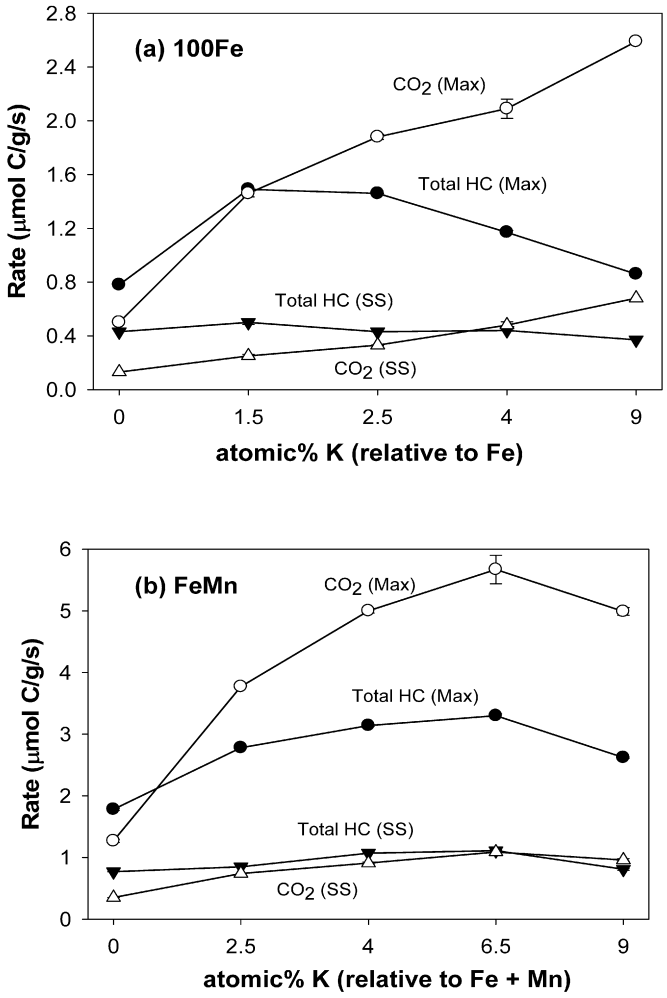


**Fig. 6.** Comparisons of the total hydrocarbon ($C_1$–$C_8$) and $CO_2$ production with %K loading for (a) 100Fe and (b) FeMn catalysts.

The influence of K level on the activities, % light olefin ($C_2$–$C_4$) selectivity, and chain growth probabilities ($\alpha$) of the Fe catalysts may be explained by a competition between CO and $H_2$ adsorption on the catalytic Fe sites. At relatively low K contents, the concentration of adsorbed H atoms is greater and chain termination via hydrogenation is more favored, which results in less olefin, shorter chain hydrocarbons and, thus, lower $\alpha$. On the other hand, as K content increases; dissociative CO adsorption is significantly enhanced, resulting in higher concentration of $-CH_2-$ species while the adsorption of $H_2$ is more hindered. Thus, the hydrogenation rate decreases, which results in higher $\alpha$ and olefin selectivity but eventually lower activity (hydrocarbon formation). A drop in FTS reaction rate for hydrocarbon products as added K exceeds an optimum level has been previously reported [1,3,11–13].

*3.2.2. SSITKA (steady state isotopic transient kinetic analysis)*

SSITKA was carried out for 100Fe, 100Fe1.5K, 100Fe2.5K, FeMn and FeMn4K to investigate the impact of K addition to precipitated Fe or to Mn-promoted Fe catalysts on the surface reaction kinetic parameters such as the intrinsic site activity and the concentration of active surface intermediates. Although FeMn6.5K exhibited the highest CO hydrogenation activity under FTS conditions, FeMn4K was chosen instead of FeMn6.5K since FeMn4K showed less Boudouard reaction with a similar CO hydrogenation activity. In order determine the cause for the differences in activity, the SSITKA study was performed for all the selected catalysts under a fixed set of methanation conditions with a $H_2$:CO ratio of 20:1 in order to obtain $CH_4$ as the primary product. Producing primarily $CH_4$ minimizes the amount of fragmentation of isotopically labeled higher hydrocarbon molecules in the mass spectrometer that can make data interpretation difficult. Although performing CO hydrogenation at a high $H_2$:CO ratio would be expected to reduce somewhat the selectivity differences between these catalysts, it can be seen by comparing Tables 3 and 4 that significant differences still remained in the impact of K promotion on the chain growth probability ($\alpha$) and % light olefin ($C_2$–$C_4$) formation. In fact, the % light olefin ($C_2$–$C_4$) formation showed an even more dramatic effect of K promotion at these conditions than at $H_2$:CO = 2.

The TOS activities of the catalysts for total hydrocarbon and $CH_4$ formation under methanation conditions are shown in Figs. 7 and 8, respectively. The formation rates of total hydrocarbon products and $CH_4$ for the FeMn catalysts were almost two times those found for the benchmark 100Fe catalyst. The addition of K to 100Fe enhanced the catalyst activity. However, 100Fe1.5K and 100Fe2.5K appeared to deactivate more significantly than 100Fe. A positive impact of K on the activity of the FeMn catalyst was also observed. The formation rates of total hydrocarbon products and $CH_4$ for FeMn4K were almost twofold those found for FeMn. However, the K-promoted FeMn did not exhibit significant deactivation showing greater catalyst stability than 100Fe1.5K or 100Fe2.5K.

The typical normalized transient response of Ar, CO and $CH_4$ is shown in Fig. 9. Detailed calculation procedures for the sur-

**Table 2**
The impact of K promotion on carbon content of the various Fe catalysts after 6 h TOS of reaction

| Catalyst[a] | Amount of carbon (mmol/g cat) | | | |
|---|---|---|---|---|
| | From Boudouard reaction[b] (calculated) | Total C deposition[c] (measured) | In form of bulk $Fe_2C_5$[d] (calculated) | Inactive carbon (coke)[e] (calculated) |
| 100Fe[f] | 0 | 4.25 | 3.73 | 0.52 |
| 100Fe1.5K | 0.01 | n/a | 3.81 | n/a |
| 100Fe2.5K | 1.10 | 5.87 | 3.81 | 2.06 |
| 100Fe4K | 1.70 | 6.47 | 3.97 | 2.51 |
| 100Fe9K | 8.97 | 8.93 | 3.97 | 4.95 |
| FeMn | 0 | 3.74 | 3.04 | 0.70 |
| FeMn2.5K | 1.32 | 5.41 | 3.25 | 2.16 |
| FeMn4K | 2.61 | n/a | 3.25 | n/a |
| FeMn6.5K | 2.70 | 6.06 | 2.93 | 3.13 |
| FeMn9K | 6.49 | 7.31 | 2.93 | 4.38 |

[a] All catalysts also contained 5Cu and 17Si.
[b] Determined by the excess amount of $CO_2$ produced from mass balance analysis between $CO_2$ formation rate and total hydrocarbon product rate curves over 6 h TOS. Max error = ±7%.
[c] Carbon content after 6 h TOS analyzed by Galbraith Lab. Max error = ±6%.
[d] Determined based upon all of Fe forming $Fe_2C_5$. The catalysts were prepared (K impregnation) from the same batch of base catalysts (100Fe or FeMn) resulting in identical amount of C for $Fe_2C_5$. Max error = ±8%.
[e] Determined from (total C deposition) − (C in bulk $Fe_2C_5$). Max error = ±10%.
[f] Initial carbon content of the fresh calcined 100Fe catalyst <0.1% (analyzed by Galbraith Lab.). Max error = ±5% of total.

**Table 3**
Catalyst activities and selectivities for the Fe-based catalysts[a]

| Catalyst[b] | %CO conversion[c] | Maximum rate[c] (μmol of C/g/s) | | SS rate[c,d] (μmol of C/g/s) | | % Hydrocarbon selectivity at SS[c,d] | | | | | % Olefins in $C_2$–$C_4$ fraction (C basis)[c,d] | $\alpha^{c,d}$ (>$C_3$) |
|---|---|---|---|---|---|---|---|---|---|---|---|---|
| | | $CO_2$ | Total HC | $CO_2$ | Total HC | $C_1$ | $C_2$ | $C_3$ | $C_4$ | $C_5$–$C_8$ | | |
| 100Fe | 1.65 | 0.50 | 0.78 | 0.13 | 0.43 | 26 | 29 | 26 | 13 | 5 | 74 | 0.35 |
| 100Fe1.5K | 2.12 | 1.49 | 1.49 | 0.25 | 0.50 | 23 | 27 | 23 | 20 | 7 | 91 | 0.35 |
| 100Fe2.5K | 2.20 | 1.86 | 1.46 | 0.3 | 0.43 | 24 | 30 | 24 | 13 | 10 | 93 | 0.46 |
| 100Fe4K | 2.55 | 2.01 | 1.17 | 0.48 | 0.44 | 19 | 25 | 22 | 16 | 17 | 95 | 0.57 |
| 100Fe9K | 3.00 | 2.59 | 0.86 | 0.68 | 0.37 | 11 | 22 | 22 | 18 | 27 | 96 | 0.61 |
| FeMn | 3.21 | 1.27 | 1.78 | 0.35 | 0.77 | 41 | 22 | 17 | 15 | 5 | 83 | 0.33 |
| FeMn2.5K | 2.34 | 3.36 | 2.78 | 0.74 | 0.85 | 27 | 27 | 25 | 13 | 8 | 93 | 0.45 |
| FeMn4K | 2.75 | 3.98 | 3.14 | 0.91 | 1.07 | 24 | 24 | 22 | 20 | 10 | 94 | 0.52 |
| FeMn6.5K | 3.24 | 3.72 | 3.30 | 1.09 | 1.11 | 22 | 25 | 20 | 15 | 18 | 97 | 0.62 |
| FeMn9K | 2.61 | 3.37 | 2.62 | 0.96 | 0.81 | 18 | 21 | 21 | 18 | 21 | 100 | 0.63 |

[a] Reaction conditions: 280 °C, 1.8 atm, $P_{H_2} = 0.3$ atm, $P_{CO} = 0.15$ atm.
[b] All catalysts also contained 5Cu and 17Si.
[c] Max error = ±5%.
[d] At steady-state rate (5 h TOS) and based on atomic carbon.

**Table 4**
Catalyst activities and selectivities for the Fe-based catalysts during SSITKA measurements[a]

| Catalyst[b] | %CO conversion[c] | Maximum rate[c] (μmol of C/g/s) | | SS rate[c,d] (μmol of C/g/s) | | % Hydrocarbon selectivity at SS[c,d] | | | | | % Olefins in $C_2$–$C_4$ fraction (C basis)[c,d] | $\alpha^{c,d}$ (>$C_3$) |
|---|---|---|---|---|---|---|---|---|---|---|---|---|
| | | $CO_2$ | Total HC | $CO_2$ | Total HC | $C_1$ | $C_2$ | $C_3$ | $C_4$ | $C_5$–$C_8$ | | |
| 100Fe | 3.60 | 0.23 | 2.47 | 0 | 1.47 | 60 | 17 | 12 | 8 | 2 | 31 | 0.38 |
| 100Fe1.5K | 3.49 | 0.66 | 4.10 | 0 | 1.79 | 54 | 18 | 13 | 10 | 4 | 61 | 0.42 |
| 100Fe2.5K | 2.96 | 0.90 | 3.37 | 0 | 1.50 | 49 | 19 | 15 | 12 | 5 | 62 | 0.45 |
| FeMn | 5.00 | 0.45 | 3.18 | 0.36 | 2.58 | 62 | 17 | 12 | 7 | 2 | 27 | 0.39 |
| FeMn4K | 5.51 | 2.33 | 5.75 | 1.28 | 4.35 | 59 | 14 | 12 | 10 | 4 | 66 | 0.46 |

[a] Reaction conditions: 280 °C, 1.8 atm, $P_{H_2} = 0.9$ atm, $P_{CO} = 0.045$ atm.
[b] All catalysts also contained 5Cu and 17Si.
[c] Max error = ±5%.
[d] At steady-state rate (5 h TOS) and based on atomic carbon.

face residence time ($\tau$) and the concentration of active surface intermediates ($N$) can be found elsewhere [19,20,33]. The average surface residence times of the intermediates leading to $CH_4$ ($\tau_{CH_4}$) were determined using SSITKA for all the catalysts. A measure of the site TOF for $CH_4$ ($TOF_{ITK}$) can be calculated from $\tau_{CH_4}$ ($TOF_{ITK} = 1/\tau_{CH_4}$). Values of $TOF_{ITK}$ for the catalysts with TOS are shown in Fig. 10. Isotopic transients for the various catalysts at steady state were all essentially identical. $TOF_{ITK}$ values increased initially with TOS and remained constant after 30 min of reaction. The intrinsic site activities for all the Fe catalysts were similar within experimental error. This implies that the average site activity was identical for all catalysts despite the presence of Mn and/or K. The increase in the value of $TOF_{ITK}$ during the initial 30 min TOS was probably due to changes in the nature of the active sites from more $Fe^0$ like to more Fe carbide like species.

Changes in the concentration of active surface intermediates leading to $CH_4$ ($N_{CH_4}$) as the reaction proceeded are shown in Fig. 11. While there were higher hydrocarbon intermediates on the surface as well during methanation, their concentration have been determined in a separate study to be small (10–20% of total hydrocarbon surface species) relative to that of methane intermediates (80–90%). As can be seen in Fig. 11, the enhanced activity caused

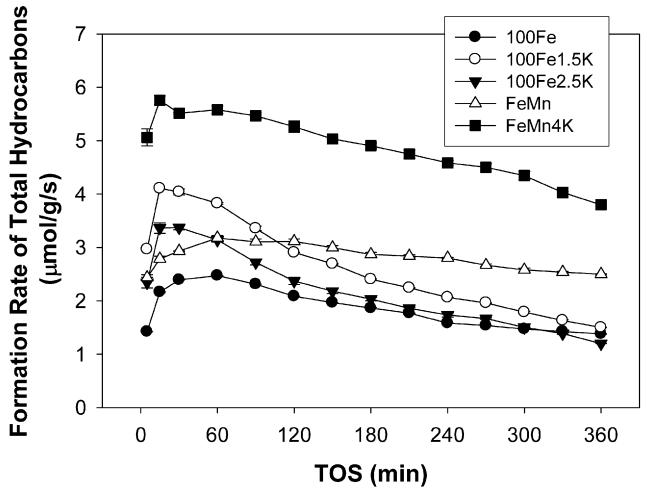


**Fig. 7.** Formation rates of total hydrocarbon products during SSITKA on the various Fe-based catalysts.

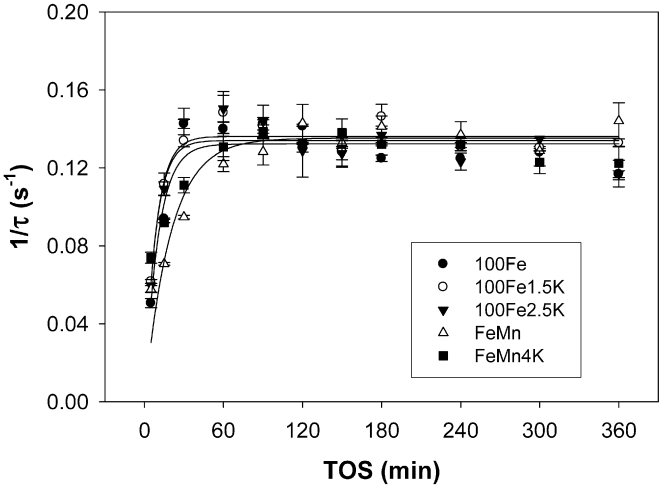


**Fig. 10.** $TOF_{ITK}$ ($1/\tau_{CH_4}$ from SSITKA) for the various Fe-based catalysts.

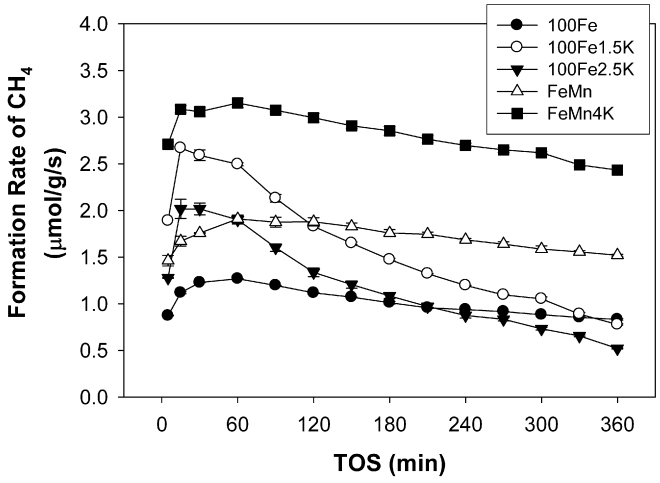


**Fig. 8.** Formation rates of $CH_4$ during SSITKA on the various Fe-based catalysts.

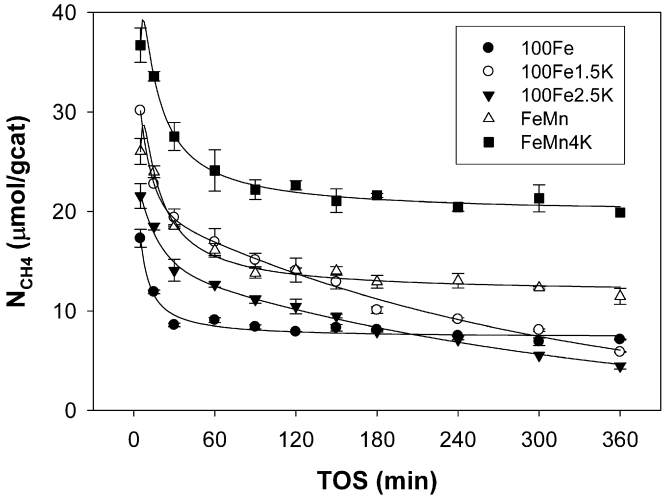


**Fig. 11.** The concentration of active surface intermediates of $CH_4$ ($N_{CH_4}$) vs TOS for the various Fe-based catalysts.

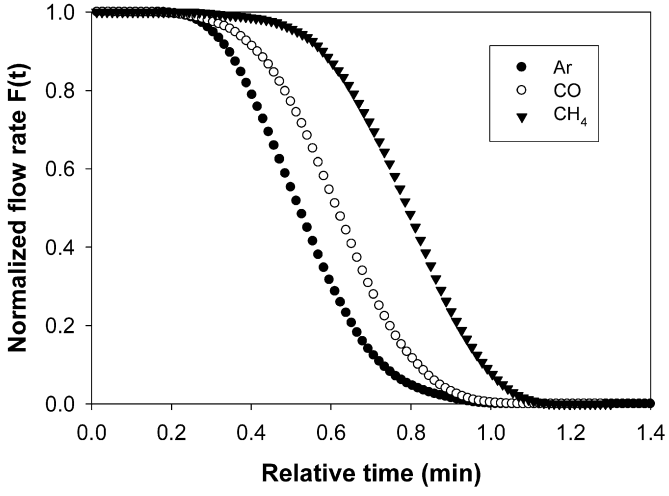


**Fig. 9.** Typical normalized transient responses of Ar (inert tracer), CO and $CH_4$ (at 280 °C and a total pressure of 1.8 atm, where $P_{H_2} = 0.3$ atm and $P_{CO} = 0.15$ atm).

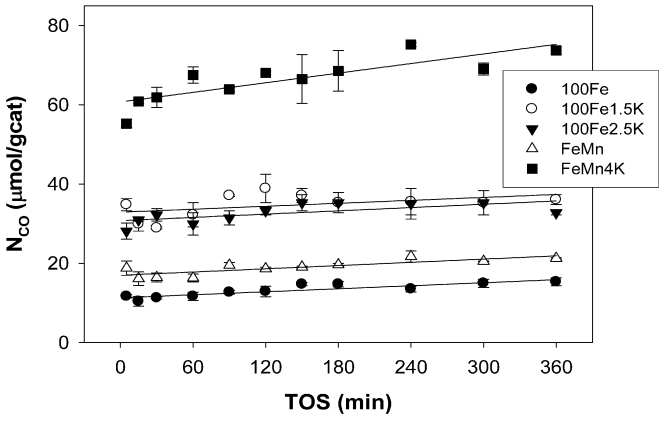


**Fig. 12.** The concentration of reversibly adsorbed CO ($N_{CO}$) vs TOS for the various Fe-based catalysts.

by the addition of Mn and/or K was primarily due to an increase in hydrocarbon surface intermediates, as indicated by $N_{CH_4}$. $N_{CH_4}$ for FeMn4K was almost 3 times higher than that for the base 100Fe catalyst. Although 100Fe1.5K and 100Fe2.5K exhibited higher $N_{CH_4}$ values initially than that of 100Fe, these $N_{CH_4}$ values decreased considerably with TOS. This suggests that significant declines in the activities of the 100Fe1.5K and 100Fe2.5K catalysts were due to a decrease in the concentration of active surface intermediates leading to $CH_4$ which was probably due to carbon deposition on the active sites. The surface concentrations during reaction of re-

versibly adsorbed CO ($N_{CO}$) (i.e., CO that adsorbed and desorbed with reacting) are shown in Fig. 12. $N_{CO}$ for 100Fe increased with the addition of Mn and was significantly enhanced by K promotion. The adsorption of CO was clearly affected by the presence of K [14,15]. Reversible adsorption of CO during reaction was not greatly affected by FTS deactivation with TOS.

## 4. Conclusion

As has previously been shown, the activities of precipitated $FeCuSiO_2$ catalysts can be improved by the addition of Mn for both CO hydrogenation and the WGS reaction. K promotion of Fe catalysts with or without added Mn enhanced the catalyst activity for both reactions in varying degrees dependent upon the K concentration. Adding K at relatively low concentrations promoted the activity of the catalysts, while the activity of catalyst declined with the addition of excess K probably in large part due to an increased amount of carbon deposition via the Boudouard reaction. Chain growth probability ($\alpha$) was enhanced as expected with the presence of K, regardless of Mn addition. The reaction site activities of the catalysts ($TOF_{ITK} = 1/\tau_{CH_4}$) as determined using SSITKA were similar, regardless of K promotion or Mn addition. On the other hand, the addition of Mn and/or K increased the concentration of active surface intermediates leading to product, which appeared to be a primary cause for the high catalytic activity observed in the K-promoted Fe and FeMn catalysts.

## Acknowledgment

This paper is based upon work supported by the National Association of State Energy Offices (NASEO) grant No. DE-FC36-03G013026.

## References

[1] R.B. Anderson, The Fischer–Tropsch Synthesis, Academic Press, Orlando, FL, 1984.
[2] http://www.energy.gov, as of February 15, 2008.
[3] M.E. Dry, The Fischer–Tropsch Synthesis, Springer-Verlag, New York, 1981, pp. 159–255.
[4] L. Bai, H.W. Xiang, Y.W. Li, Y.Z. Han, B. Zhong, Fuel 81 (2002) 1577–1581.
[5] C. Wang, Q.X. Wang, X.D. Sun, L.Y. Xu, Catal. Lett. 105 (2005) 93–101.
[6] W. Ma, E.L. Kugler, J. Wright, D.B. Dadyburjor, Energy Fuels 20 (2006) 2299–2307.
[7] T.C. Bromfield, R. Visagie, U.S. Patent WO2005/049765A1, 2005.
[8] N. Lohitharn, J.G. Goodwin Jr., E. Lotero, J. Catal. 255 (2008) 104–113.
[9] K.B. Jensen, F.E. Massoth, J. Catal. 92 (1985) 109–118.
[10] T.Z. Li, Y. Yang, C.H. Zhang, X. An, H.J. Wan, Z.C. Tao, H.W. Xiang, Y.W. Li, F. Yi, B.F. Xu, Fuel 86 (2007) 921–928.
[11] Y. Yang, H.W. Xiang, Y.Y. Xu, L. Bai, Y.W. Li, Appl. Catal. A Gen. 266 (2004) 181–194.
[12] D.B. Bukur, D. Mukesh, S.A. Patel, Ind. Eng. Chem. Res. 29 (1990) 194–204.
[13] D.G. Miller, M. Moskovits, J. Phys. Chem. 92 (1988) 6081–6085.
[14] M.E. Dry, T. Shingles, L.J. Boshoff, G.J. Oosthuizen, J. Catal. 15 (1969) 190–199.
[15] I.M. Campbell, Catalysis at Surfaces, Chapman and Hall, New York, 1988, p. 133.
[16] Z.C. Tao, Y. Yang, H.J. Wan, T.Z. Li, X. An, H.W. Xiang, Y.W. Li, Catal. Lett. 114 (2007) 161–168.
[17] D.B. Bukur, X.S. Lang, J.A. Rossin, W.H. Zimmerman, M.P. Rosynek, E.B. Yeh, C.P. Li, Ind. Eng. Chem. Res. 28 (1989) 1130–1140.
[18] H.J. Jung, M.A. Vannice, L.N. Mulay, R.M. Stanfield, W.N. Delgass, J. Catal. 76 (1982) 208–224.
[19] J.G. Goodwin Jr., S.Y. Kim, W.D. Rhodes, in: J.J. Spivey, G.W. Roberts (Eds.), Catalysis, The Royal Society of Chemistry, 2003, Chapter 8.
[20] S. Hammache, J.G. Goodwin Jr., S.L. Shannon, S.Y. Kim, in: Encyclopedia of Surface and Colloid Science, vol. 1, 2002, pp. 2445–2454.
[21] N. Lohitharn, J.G. Goodwin Jr., J. Catal. (2008), submitted for publication.
[22] S.Z. Li, S. Krishnamoorthy, A.W. Li, G.D. Meitzner, E. Iglesia, J. Catal. 206 (2002) 202–217.
[23] R. Brown, M.E. Cooper, D.A. Whan, Appl. Catal. 3 (1982) 177–186.
[24] D.B. Bukur, C. Sivaraj, Appl. Catal. A Gen. 231 (2002) 201–214.
[25] J.L. Rankin, C.H. Bartholomew, J. Catal. 100 (1986) 533–540.
[26] K.B. Jensen, F.E. Massoth, J. Catal. 92 (1985) 98–108.
[27] M.D. Lee, J.F. Lee, C.S. Chang, T.Y. Dong, Appl. Catal. 72 (1991) 267–281.
[28] C. Rhodes, B.P. Williams, F. King, G.J. Hutchings, Catal. Commun. 3 (2002) 381–384.
[29] S.Z. Li, R.J. O'Brien, G.D. Meitzner, H. Hamdeh, B.H. Davis, E. Iglesia, Appl. Catal. A Gen. 219 (2001) 215–222.
[30] J.W. Niemantsverdriet, A.M. van der Kraan, W.L. van Dijk, H.S. van der Baan, J. Phys. Chem. 84 (1980) 3363–3370.
[31] W.S. Ning, N. Koizumi, H. Chang, T. Mochizuki, T. Itoh, M. Yamada, Appl. Catal. A Gen. 312 (2006) 35–44.
[32] H. Arakawa, A.T. Bell, Ind. Eng. Chem. Process Des. Dev. 22 (1983) 97–103.
[33] S.L. Shannon, J.G. Goodwin Jr., Chem. Rev. 95 (1995) 677–695.